1997

# Semiclassical Picture of Collision-induced Λ-doublet Transitions in Diatomic Molecules

Laurie J. Kovalenko

J. B. Delos
*William & Mary*, jbdelo@wm.edu



## Recommended Citation

Kovalenko, Laurie J. and Delos, J. B., Semiclassical Picture of Collision-induced Λ-doublet Transitions in Diatomic Molecules (1997). *Journal of Chemical Physics*, 107(14), 5473-5487. https://doi.org/10.1063/1.474252

# Semiclassical picture of collision-induced Λ-doublet transitions in diatomic molecules

Laurie J. Kovalenko
*Natural Sciences Collegium, Eckerd College, St. Petersburg, Florida 33711*

John B. Delos
*Physics Department, College of William and Mary, Williamsburg, Virginia 23185*

(Received 4 February 1997; accepted 26 June 1997)

We investigate collision-induced Λ-doublet transitions in a system similar to NO+Ar, based on a semiclassical model in which nuclear motion is treated classically and electronic motion quantum mechanically. We present a picture of this process by monitoring $\langle\Lambda\rangle$, the expectation value of the projection of electronic orbital-angular momentum onto the molecular NO axis, over the duration of the collision. In a typical collision, the interaction with Ar would cause the electronic orbital-angular momentum to precess about the rotating NO–Ar vector. However, since this angular momentum is locked tightly to the diatomic axis, it is restricted to oscillation along this axis. This oscillation leads to transitions between Λ-doublet states. In addition to providing this physical picture of the collision process, we calculate an alignment effect of 1.2 for a hypothetical three-vector correlation experiment, neglecting spin. © *1997 American Institute of Physics.* [S0021-9606(97)02037-0]

## I. INTRODUCTION

The goal of this work is to understand the mechanism of collision-induced Λ-doublet transitions in diatomic molecules. Using a semiclassical model, we provide a physical picture of the collision by generating Vector Evolution Diagrams, i.e., snapshots of the expectation value of the electronic orbital-angular momentum vector, $\langle\mathbf{L}\rangle$, along the course of a trajectory. We compare the behavior of a molecular collision system, NO+Ar, to that of an analogous atomic collision system,[1] Na+He, and find the transition mechanism to be analogous. For an atomic collision system such as Na +He, $\langle\mathbf{L}\rangle$ locks onto and rapidly precesses about the internuclear axis. In a molecular system such as NO+Ar, $\langle\mathbf{L}\rangle$ is strongly coupled to the diatomic NO axis. As the perturber (Ar) approaches, we might expect $\langle\mathbf{L}\rangle$ to precess about the NO–Ar vector, but the coupling is too weak to unlock $\langle\mathbf{L}\rangle$ from the diatomic NO axis. Hence the motion of $\langle\mathbf{L}\rangle$ is a restricted precession; it oscillates along the diatomic axis.

In addition to providing this physical picture, we investigate how collision alignment affects the probability for a Λ-doublet transition. Two different collision alignments are shown schematically in Fig. 1. In (a) the collision partner approaches perpendicular to the Π-orbital, and parallel to the diatomic axis, while in (b) it approaches parallel to the orbital, and perpendicular to the diatomic axis.

Experiments have shown that the orbital alignment of atoms [for instance, Ca (Ref. 2) and Ne** (Ref. 3)] with respect to the relative velocity vector can have a large effect on the outcome of a collision. We know of no analogous experiments which explore the effect of alignment or orientation of the Λ-doublet state with respect to the initial velocity vector, though Stolte and co-workers[4] mention such an idea as their next step. We discuss such a hypothetical experiment below.

Preferential population of one component of a Λ-doublet has been observed in many collision experiments. (For a recent review see Dagdigian.[5]) Although the energy difference between two Λ-doublet states is small, typically less than $1\ \mathrm{cm}^{-1}$, there is a big difference between the states in the spatial orientation of their electronic wave functions (as seen in previous paper, Fig. 1). Thus preferential population of one component over the other may provide clues about the dynamics of the collision.

We first mention experiments in which the initial state, before collision, is prepared in a single component of a Λ-doublet. The first study of collisionally-induced electronic energy transfer in $^1\Pi$ diatomic molecules was reported in 1970 by Zare and co-workers,[6] in which they irradiated a mixture of $Li_2$ dimer and Ar and monitored the resulting fluorescence spectrum. For collisions in which there is both a transition between Λ-doublet states and a change in the molecule's rotational quantum number by one quantum, they found that there is a strong preference for that quantum number to increase if the molecule is initially in one Λ-doublet state, but to decrease if the molecule is initially in the other Λ-doublet state. They proposed a transition mechanism, based on a simple, billiard-ball-like classical model, in which the observed propensities could be explained by the difference in the spatial distribution of the electron charge density for the two Λ-doublet states. Also using laser-induced fluorescence, Bergmann and Demtröder[7] investigated collision-induced transitions in the $Na_2$ dimer with many different collision partners, and found similar propensity rules. Moreover, they saw a reversal in the propensities for heavier rare gas collision partners. They proposed a different transition mechanism based on a qualitative semiclassical model, in which the potential energy curves would split as the collision partners neared each other. Bergmann *et al.*[8] used the Born approximation and found that this model also predicted the observed propensities. Poppe[9] extended the theoretical study to symmetric top molecules in general and provided a physical interpretation of the observed propensities based on

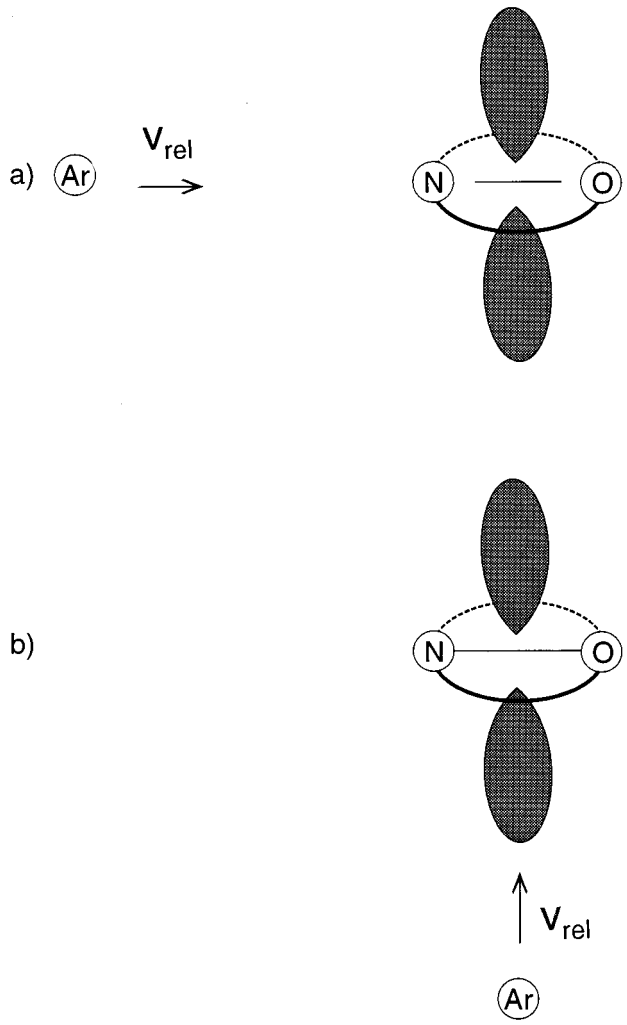


FIG. 1. Schematic of two alignments for collision-induced Λ-doublet transition. In both (a) and (b), the initially prepared electronic orbital, indicated by the shaded region, is perpendicular to the diatomic plane of rotation, indicated by the curved line. In (a) the relative velocity vector is perpendicular to the electronic orbital and parallel to the diatomic axis, while in (b) the relative velocity vector is parallel to the orbital and perpendicular to the diatomic axis.

quantum-mechanical interference. Ottinger[10] extended experimental studies to the lower-symmetry NaLi dimer, found similar propensities, and showed that these results too were in agreement with the predictions of a quantum theory using the Born approximation. Klar and Klar[11] performed a quantum calculation of the $Na_2+He$ system, using a strong coupling approximation. More recently, Lemoine *et al.*[12] used a close-coupled quantum calculation of the $Li_2$ dimer collision with He and Ne; their predictions agree well with the observed propensities, which they also conclude are a direct manifestation of quantum interference effects.

We now consider experiments on systems other than alkali dimers in which the initial state is produced in a single Λ-doublet. Copeland and Crosley[13] used a laser to prepare OH in a single state of a Λ-doublet and then used another laser to probe the states produced by collision with $H_2O$. For the rotationally inelastic collision in which $J=3/2\rightarrow J=5/2$, they saw that transition into a particular Λ-doublet state, the one conserving the $e/f$ label, was favored by a factor of 2.7. This experiment was done in a flow cell and thus did not distinguish between collisions differing in alignment. In a similar study,[14] Crosley and co-workers measured cross sections for collision of OH with He and found, for spin–orbit changing collisions, not conservation of $e/f$ label, as was seen in the case with collision with $H_2O$, but conservation of total parity; their results agreed with quantum scattering calculations. More recently, Schreel *et al.* measured parity-resolved state-to-state cross sections for rotational excitation of OH by collision with the rare gases He and Ar,[15] and with $H_2$,[16] using a crossed molecular-beam apparatus in conjunction with a hexapole electric field. Quantum calculations of these collisions systems using the coupled-states approximation were done by Offer *et al.*,[17] and Esposti *et al.*[18]

To study rotational energy transfer for collision of a single Λ-doublet state of CaF with rare gases, Dufour *et al.*[19] used a pump–probe technique, averaging over all collision orientations, and found a propensity for electronic parity conservation, in agreement with theoretical predictions. Using an optical–optical double resonance technique, Norman and Field[20] also studied the CaF+Ar system, extending the study to include collision-induced angular momentum reorientation. They too saw a propensity for parity conservation in transitions between Λ-doublet states.

Recently, Stolte and co-workers[4] measured state-to-state cross sections for rotationally inelastic collisions of a single Λ-doublet state of NO with Ar using crossed beams and a hexapole state selection technique. They saw propensity for electronic parity-conserving transitions. Though they did not measure the effect of NO orientation on the transitions, they did say that such an experiment will be their next step.

We now mention studies in which preferential population of a Λ-doublet state doublet state was seen even though the initial states were in a statistical mixture of Λ-doublet states. In 1976 Bertojo *et al.*[21] used a semiclassical model to predict preferential population of one Λ-doublet over the other in the collision of CH and OH molecules with H, $H_2$, and He. Their motivation was to find a mechanism responsible for observed maser action coming from outer-space. More recently, experiments have been performed in the laboratory demonstrating preferential population. Andresen *et al.*[22] studied $OH+H_2$ using a crossed-beam apparatus and found that the unpaired $\pi$ orbital ends up preferentially aligned *in the plane* of rotation of the OH product. Macdonald and Liu[23] investigated the inelastic scattering of CH ($X\ ^2\Pi$) with He and found in this case that the $\pi^1$ electronic orbital preferentially ends up *perpendicular to the plane* of rotation of the product CH. The difference between these two systems is attributed to the former being a $\pi^1$ system while the latter is a $\pi^3$ system. Full quantum calculations for the CH and OH systems have been done by Schinke and Andresen,[24] Dagdigian *et al.*,[25] and by Miller *et al.*[26] and the results show good agreement with experiment. Andresen *et al.*[27] took another look at the $OH+H_2$, $D_2$ system and concluded that this collision system is not a possible pump mechanism for the OH maser.

Joswig *et al.*[28] used a similar type of crossed-molecular

beam experiment to study the NO+rare gas system, with the NO prepared in a statistical mixture of Λ-doublet states. They looked for preferential population of one Λ-doublet state over the other, but none was observed. Corey and Alexander[29] also modeled these experiments, using the infinite-order sudden approximation, and found good agreement for collision with He though not so good for collision with Ar. Using a very different experimental technique, that of Direct Ion Imaging, Houston and co-workers[30] measured differential cross sections for the NO+Ar system, but they did not resolve final Λ-doublet states. Gentry and co-workers[31] also obtained differential cross sections for the NO+Ar collision system, using crossed beams and laser-induced fluorescence and found preferential population of final Λ-doublet states. Alexander[32] modeled both groups' experiments using new *ab initio* potential energy surfaces and found good agreement in general. In addition, he found a tendency for population of particular final Λ-doublet states with $\Pi(A'')$ reflection symmetry.

Here we consider a simplified model of a collision system similar to NO+Ar. We develop a semiclassical theory and an intuitive picture of the dynamics of such collisions, and we investigate how the alignment of the electronic Π orbital affects the probability for a Λ-doublet transition. To keep our description as simple as possible, we ignore two aspects of the behavior of this system, electron spin and molecular rotation during the collision with the perturber. Since we neglect electron spin, our description is good for a diatomic in a $^1\Pi$ state (NO is a $^2\Pi$); in a future paper, we plan to incorporate the effects of spin. There are two justifications for neglecting molecular rotation during the collision. First, often in experiments (especially with He as the perturber) the collision time is much less than the rotation time. Second, it is now possible to devise experiments in which a diatomic molecule is nearly oriented, its axis librating about a fixed direction. For instance, Friedrich *et al.*[33] used a strong electric field to create ''pendular'' states which librate about the direction of the applied field. Using this technique in a crossed molecular beam apparatus, the diatomic axis could thus be prepared parallel to or perpendicular to the relative velocity vector of the collision partners. A laser could be used to prepare the initial electronic state before collision; to prepare an initial electronic state with $\Lambda=+1$ a circularly polarized laser could be used, while to prepare a $\Pi_x$ orbital a linearly polarized laser could be used. Collision might then cause a transition from the initial $\Lambda=+1$ to the $\Lambda=-1$ state, or from an initial $\Pi_x$ state to the $\Pi_y$ state. Then the final state could be detected by fluorescence. For such a hypothetical experiment, we calculate the alignment effect, the ratio of the cross section for $\mathbf{v}_{\rm rel}$ parallel vs perpendicular to the diatomic axis. We hope our results encourage future experiments.

In Sec. II we review our semiclassical model for the diatomic molecule and modify it with further approximations appropriate for the particular system studied here. In Sec. III we describe our semiclassical scattering theory and in Secs. IV and V we present our results, vector evolution diagrams and alignment effect. In Sec. VI we present approximate analytic solutions to this model, and compare their predictions to those of our numerical model, providing further physical insight into the mechanism. We show that for some orientations there is, in addition to a locking region, an interior unlocking region. In Sec. VII we summarize our conclusions.

## II. MODEL FOR DIATOMIC

In the preceding paper, we presented a semiclassical model for a diatomic molecule and compared the results to those of a full quantum theory. Here we use the semiclassical model for our model molecule, spinless NO. In the semiclassical model, the two nuclei are treated classically and the active electron is treated quantum mechanically. We use a rigid rotor approximation, fixing the NO bond length at the equilibrium separation, and use the Born–Oppenheimer electronic basis, truncating this set to the three basis states having $L=1$, which are the two Π states and one Σ state. Parameters needed for the calculation are[34] the difference in energy between the Π and Σ electronic states, $\Delta\epsilon_{\Sigma,\Pi}=44\,000\ \mathrm{cm}^{-1}$, the bond length, $R=1.23$ Å, and the rotational constant, $B=1.7\ \mathrm{cm}^{-1}$. This gives a ratio, $\Delta\epsilon_{\Sigma,\Pi}/B$, of 26 000, which indicates $\langle\mathbf{L}\rangle$ is locked tightly onto the diatomic axis.

Figure 2 shows vector evolution diagrams, snapshots of $\langle\mathbf{L}\rangle$ along the course of a trajectory, for an isolated, rotating, NO molecule both in the space-fixed frame and in the rotating frame. The initial electronic state is $\Lambda=-1$. From Fig. 2(a) we see that the molecule rotates about 3/4 of the way in 1 ps, during which time $\langle\mathbf{L}\rangle$ rotates right along with the diatomic axis. From Fig. 2(b) we see that $\langle\mathbf{L}\rangle$ is locked tightly onto the molecular axis.

Figure 3 shows the behavior of $\langle\mathbf{L}\rangle$ in the presence of a perturber, an Ar atom, located along the $Z^L$ axis at a distance of 6 a.u. from the diatomic. We see that the perturber causes $\langle\mathbf{L}\rangle$ to oscillate along the diatomic axis, yet remain tightly locked onto that axis. Thus we conclude that the role of the Σ state in the collision dynamics is negligible for this collision system, and we consider only two states, $\Lambda=\pm1$ (or, equivalently, $\Pi_X$ and $\Pi_Y$).

## III. SCATTERING THEORY

We model a hypothetical crossed-beam experiment in which the NO diatomic axis is oriented in the plane of the macroscopic beams, either parallel or perpendicular to the average relative velocity vector, $\mathbf{v}_{\rm rel}$ and the molecule is then prepared either in the electronic Π state, aligned in the plane of the macroscopic beams, or in the electronic $\langle\Lambda\rangle=+1$ state. Our approach is similar to that used in a previous paper[1] for the Na+He collision system, where the nuclear motion was treated with classical mechanics and the electronic motion with quantum mechanics, except that now we have three nuclei, rather than two.

### A. Frames of reference

We define a space-fixed lab frame $(X^L,Y^L,Z^L)$, shown in Fig. 4(a), taking $Z^L$ along $\mathbf{v}_{\rm rel}$, $X^L$ in the plane defined by

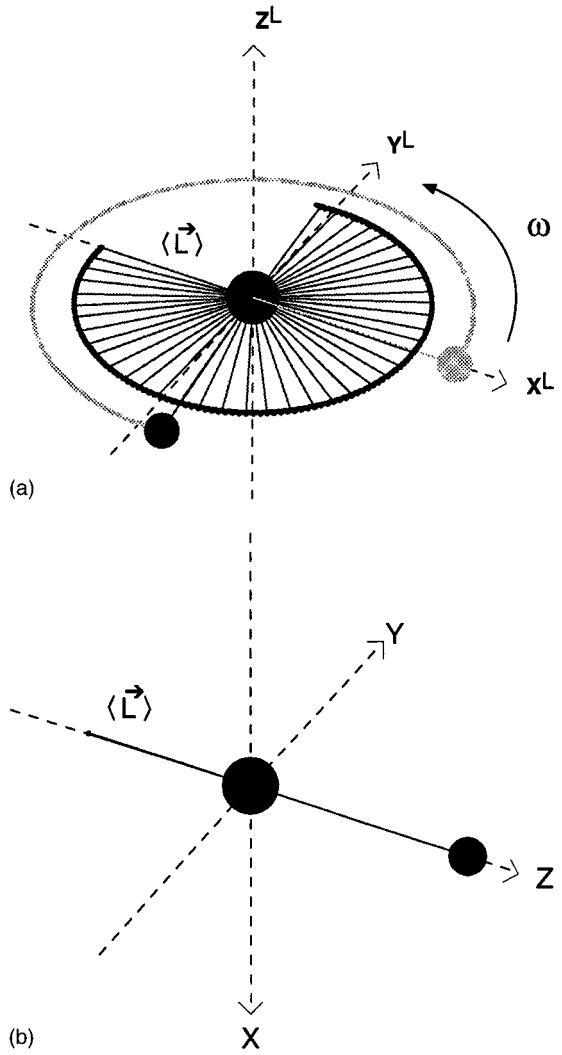


FIG. 2. Vector evolution diagrams of $\langle \mathbf{L} \rangle$, for an isolated NO molecule with low rotation ($K=7$). A two-dimensional trajectory is used. (a) A typical trajectory is shown in the space-fixed laboratory frame with the N atom at the origin. The initial position of the O atom is shown in gray, the final position in black, from which it is seen that the molecule undergoes about 3/4 of a rotation in 1 ps. Several snapshots of the vector $\langle \mathbf{L} \rangle$ are shown. The heavy black line shows the locus of the tips of this vector, which starts out along the negative $X^L$ axis and ends up along the positive $Y^L$ axis. (b) The same trajectory is shown but in the rotating (body-fixed) frame. It is evident that $\langle \mathbf{L} \rangle$, which starts out along the internuclear axis (pointing along the negative $Z$ axis), remains ''locked'' to that axis. Since for a $\Sigma$ state $\langle \mathbf{L} \rangle$ is perpendicular to the internuclear axis, we conclude that the contribution of the $\Sigma$ state is negligible.

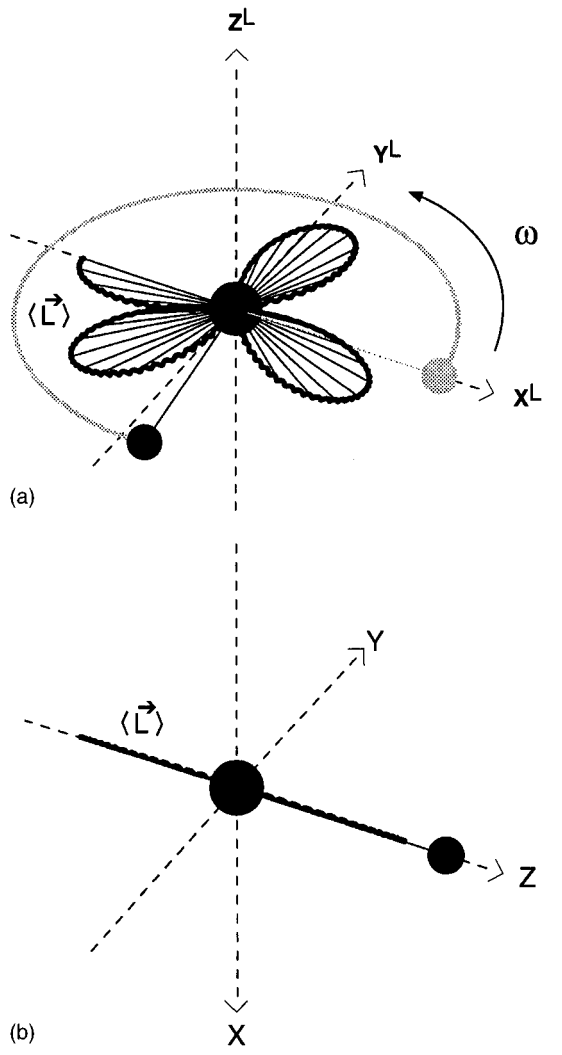


FIG. 3. Same as Fig. 2 except that now there lies a perturber atom, Ar, located 6 a.u. away along the $Z^L$ axis. We see that the effect of the perturber is to cause $\langle \mathbf{L} \rangle$ to oscillate along the internuclear axis.

the two macroscopic beams, and $Y^L$ so as to complete a right-handed coordinate system. We put the origin at the center of mass of the diatomic molecule.

For each individual collision, the position of the perturbing atom, Ar, is defined by the coordinates $R$, $\Theta^L_{\mathrm{Ar}}$, and $\Phi^L_{\mathrm{Ar}}$ as shown in Fig. 4(b). We define a space-fixed collision frame, $X'$, $Y'$, $Z'$, where $Z'$ is along $Z^L$, $X'$ is obtained by projecting $\mathbf{R}^L_{\mathrm{Ar}}$ onto the $X^L$, $Y^L$ plane, and $Y'$ is chosen to complete a right-handed coordinate system. Since the experiment would not distinguish between collisions differing in the azimuthal angle, $\Phi^L_{\mathrm{Ar}}$, about $\mathbf{v}_{\mathrm{rel}}$, nor between collisions differing in impact parameter, $b$, we average over these parameters to calculate cross sections for electronic transitions.

For an individual collision, the state of the diatomic NO molecule is characterized by the internuclear vector $\mathbf{R}$, which is oriented with an electric field along either the $X^L$ or the $Z^L$ axis. The state of the diatomic molecule is then characterized by $R$ and $\beta$, as shown in Fig. 4(c), where $\beta$ is the angle between $Z^L$ and $\mathbf{R}$. In the kind of experiment discussed here, in which the NO molecule is oriented by an external field, $\beta$ can be continuously adjusted experimentally from 0 to $\pi$. In our present calculations, we consider the two cases $\beta=0$ and $\beta=\pi/2$, so NO is either along the $Z^L$ axis (parallel to $\mathbf{v}_{\mathrm{rel}}$) or along the $X^L$ axis (perpendicular to $\mathbf{v}_{\mathrm{rel}}$).

We now define a space-fixed diatomic frame, $X$, $Y$, $Z$, where $Z$ is along $\mathbf{R}$, $X$ is defined by rotation of $X^L$ by $\beta$, and $Y$ is chosen to complete a right-handed coordinate frame. This choice of diatomic frame is consistent with that in the preceding paper. We need one more frame of reference, the ''rotating triatomic'' frame of reference, $X^T$, $Y^T$, $Z^T$. The position of Ar in the diatomic frame, specified by $R_{\mathrm{Ar}}$, $\Theta_{\mathrm{Ar}}$, and $\Phi_{\mathrm{Ar}}$ as shown in Fig. 4(d), defines the rotating triatomic

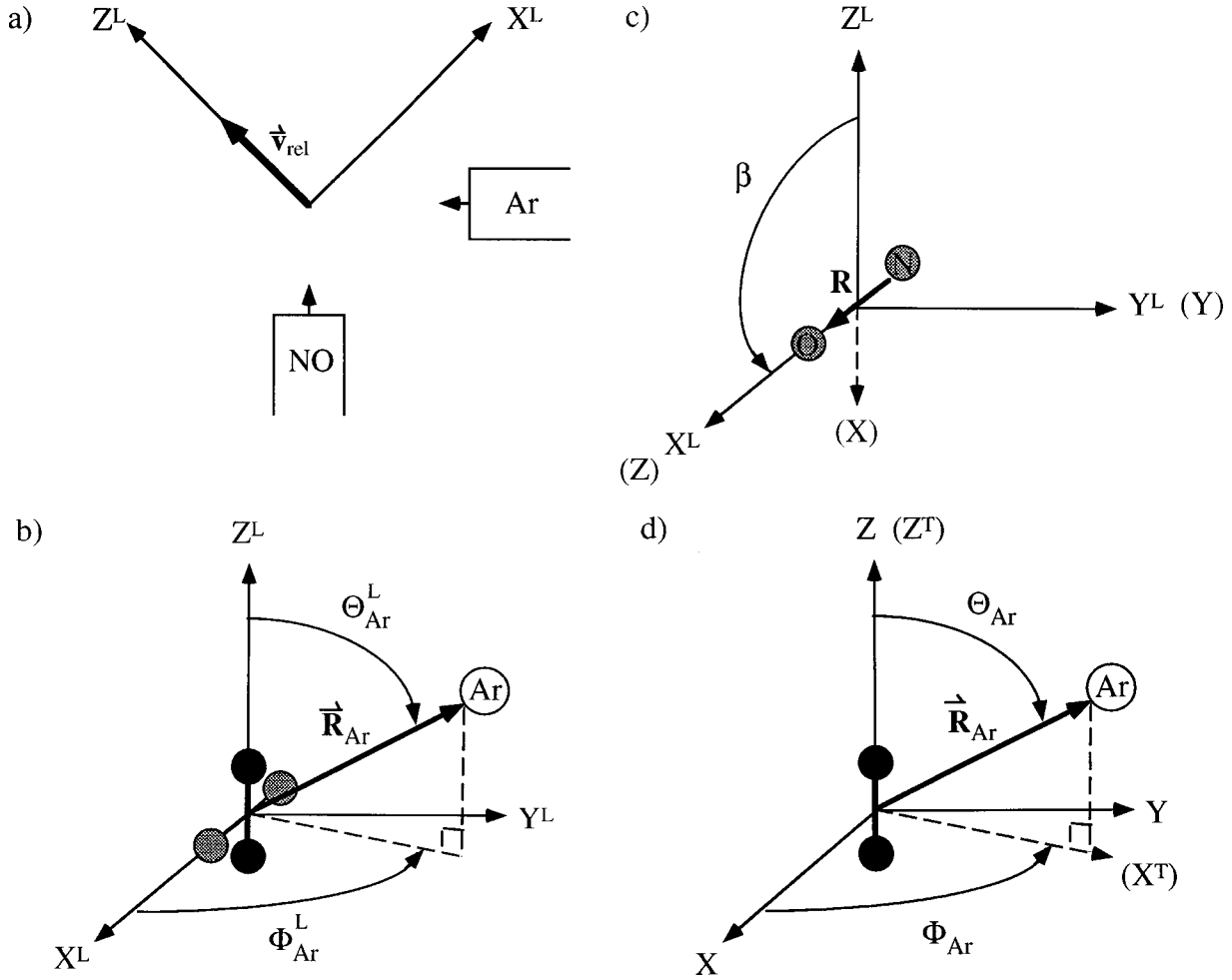


FIG. 4. (a) Laboratory frame $(X^L,Y^L,Z^L)$. The plane of the two macroscopic molecular beams defines the $X^L$, $Z^L$ plane, with $Z^L$ in the direction of Ar relative to NO. The $Y^L$ axis is then chosen to complete a right-handed coordinate frame. (b) Collision frame $(X',Y',Z')$. The NO molecule is shown as either the black or the gray circles, corresponding to alignment either along the $Z^L$ axis or along the $X^L$ axis, respectively. The $X'$ axis is defined by the projection of $\mathbf{R}_{\mathrm{Ar}}$ onto the $X^L$, $Y^L$ plane. $\Phi^L_{\mathrm{Ar}}$ is the azimuthal angle for $\mathbf{R}_{\mathrm{Ar}}$. To calculate cross sections, we average over $\Phi^L_{\mathrm{Ar}}$ and impact parameter, $b$. (c) Diatomic frame (space-fixed for the case considered here of an oriented molecule) defined by the orientation of molecule NO in lab frame. For the case considered here, the diatomic axis, $\mathbf{R}$, pointing from N to O, is restricted to lie in the $X^L$, $Y^L$ plane, with $\beta$ the angle between $Z^L$ and $\mathbf{R}$. The $Z$ axis is defined along $\mathbf{R}$, and rotation of $X^L$ by $\beta$ defines $X$. The $Y$ axis is then chose to complete a right-handed coordinate system. (d) Triatomic frame (rotating) defined by position of Ar in diatomic frame. $Z^T$ is taken along $Z$, $X^T$ is defined by the projection of $\mathbf{R}_{\mathrm{Ar}}$ onto the $X$, $Y$ plane, and $Y^T$ (not shown) chosen so as to complete a right-handed coordinate system.

frame, where $Z^T$ is taken along $Z$, $X^T$ is obtained by rotating the $X$ axis about $Z^T$ by $\Phi_{\mathrm{Ar}}$, and $Y^T$ is chosen to complete a right-handed coordinate frame. The rate of rotation of the triatomic frame is thus defined by $d\Phi_{\mathrm{Ar}}/dt$. If $\beta=0$, and the NO axis coincides with the $Z^L$ axis, $\Phi_{\mathrm{Ar}}$ is constant, and the ''rotating triatomic'' frame has zero rotation rate. For nonzero $\beta$, the rotation rate does not vanish, and couplings associated with the rotation of the frame enter the Hamiltonian.

The potential-energy surfaces are defined in this ''rotating triatomic'' frame. One electronic state ($A'$ or ''ip'') has the Π orbital in the plane of the triatomic, while the other ($A''$ or ''op'') has the Π orbital perpendicular to the plane.

### B. Schrödinger equation for electronic motion

The Schrödinger equation for the active electron is given by

$$i\hbar\,\frac{\partial\Psi[\mathbf{r};\mathbf{R}_{\mathrm{Ar}}(t)]}{\partial t}=h_{\mathrm{el}}\Psi[\mathbf{r};\mathbf{R}_{\mathrm{Ar}}(t)], \tag{1}$$

where $\mathbf{r}$ and $\mathbf{R}_{\mathrm{Ar}}(t)$ are vectors representing the position of the electron and argon atom, respectively, relative to the center of mass of the NO molecule. The length and direction of $\mathbf{R}_{\mathrm{Ar}}(t)$ in the laboratory frame are defined by the spherical coordinates $[R_{\mathrm{Ar}}(t),\ \Phi^L_{\mathrm{Ar}}(t),$ and $\Phi^L_{\mathrm{Ar}}(t)=\Phi^L_{\mathrm{Ar}}(0)]$, as shown in Fig. 4(b). Since we are suppressing electronic spin, we consider only the electrostatic part of the Hamiltonian, $h_{\mathrm{el}}$, called the ''Born–Oppenheimer Hamiltonian,'' and given by

$$h_{\mathrm{el}}=\frac{-\hbar^2}{2m}\,\nabla_r^2+V_{e-,\mathrm{N}+}+V_{e-,\mathrm{O}}+V_{e^-,\mathrm{Ar}}. \tag{2}$$

We reduce the Schrödinger equation to a set of coupled equations by expanding $\Psi$ in a basis

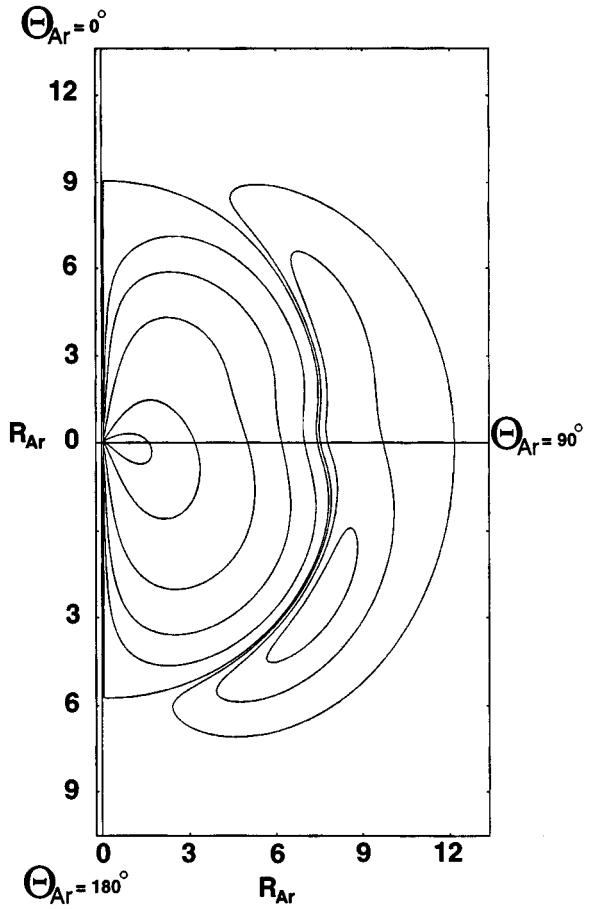


FIG. 5. A contour plot of the anisotropy, $\Delta\epsilon_{\mathrm{ip,op}}$, for the NO+Ar system, generated from a calculation by Nielson *et al.* The N and O atoms lie on the axis as shown, and the contours give the value of $\Delta\epsilon_{\mathrm{ip,op}}$ for a given position ($R_{\mathrm{Ar}}$ and $\theta_{\mathrm{Ar}}$) of Ar. All units are atomic units.

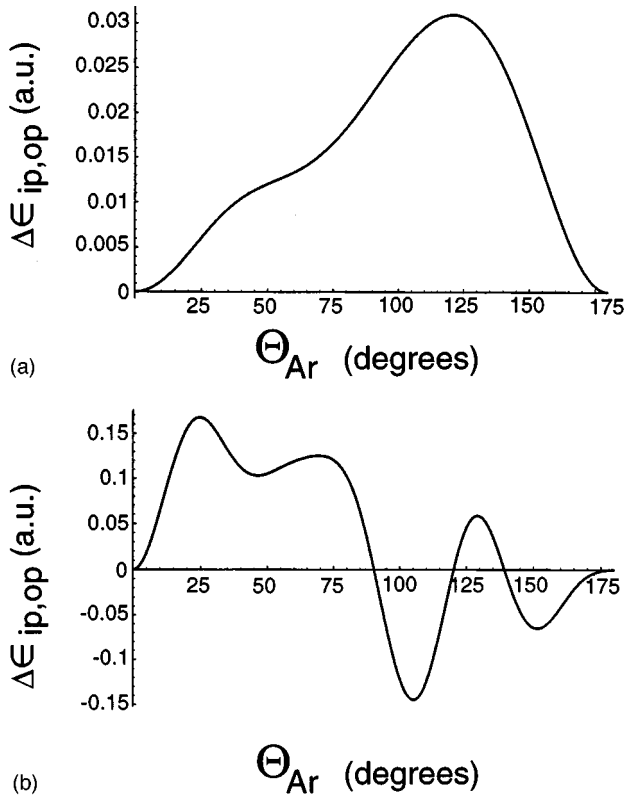


FIG. 6. A plot of the anisotropy of the potential, $\Delta\epsilon_{\mathrm{ip,op}}$, as a function of angle, $\Theta_{\mathrm{Ar}}$, as defined in Fig. 5 for a fixed internuclear distance of 3 a.u. using (a) potential energy surfaces calculated by Nielson *et al.*, and (b) potential energy surfaces calculated by Alexander. Since we expect a smooth variation with angle, we have chosen to use the potential energy surfaces of Nielson *et al.* for our scattering calculation.

$$\Psi(\mathbf{r},t)=\sum_k c_k(t)\,\phi_k[\mathbf{r};\mathbf{R}_{\mathrm{Ar}}(t)], \tag{3}$$

where we choose as basis functions the Born–Oppenheimer electronic eigenfunctions, $\phi_k[\mathbf{r};\mathbf{R}_{\mathrm{Ar}}(t)]$, which satisfy

$$h_{\mathrm{el}}\phi_k[\mathbf{r};\mathbf{R}_{\mathrm{Ar}}(t)]=\epsilon_k\phi_k[\mathbf{r};\mathbf{R}_{\mathrm{Ar}}(t)]. \tag{4}$$

We truncate this basis set to the two diatomic molecular states having $L=1$ and $\Lambda=\pm1$ symmetry with respect to the diatomic molecular axis, or $Z$ axis. (This truncation is a good one, as shown in Sec. II above, since the $\Sigma$ state is 44 000 $\mathrm{cm}^{-1}$, higher in energy than the $\Pi$ states.) As stated before, the plane of the triatomic is a plane of symmetry, so the two eigenstates are $\phi_{\mathrm{ip}}$ (in-plane or $A'$) and $\phi_{\mathrm{op}}$ (out-of-plane or $A''$). These are linear combinations of the states of definite $\Lambda$. We take the energies of these states to be those of the NO–Ar system.

The eigenvalues, $\epsilon_{\mathrm{ip}}(R_{\mathrm{Ar}},\Theta_{\mathrm{Ar}})$ and $\epsilon_{\mathrm{op}}(R_{\mathrm{Ar}},\Theta_{\mathrm{Ar}})$, have been calculated by Nielson *et al.*[35] Since the transition probability is mainly determined by the anisotropy of the potential, characterized by $\Delta\epsilon_{\mathrm{ip,op}}=(\epsilon_{\mathrm{ip}}-\epsilon_{\mathrm{op}})$, we show a contour plot of $\Delta\epsilon_{\mathrm{ip,op}}$ in Fig. 5. More recently, Alexander[32] has calculated these surfaces using a different method. Figure 6 shows plots of $\Delta\epsilon_{\mathrm{ip,op}}$ vs $\Theta_{\mathrm{Ar}}$ at fixed $R_{\mathrm{Ar}}$ for both calculations. As there is a small difference between $\epsilon_{\mathrm{ip}}(R_{\mathrm{Ar}},\Theta_{\mathrm{Ar}})$ and $\epsilon_{\mathrm{op}}(R_{\mathrm{Ar}},\Theta_{\mathrm{Ar}})$, it is hard to calculate this difference. We chose the older calculation, shown in Fig. 6(a), over the newer one, shown in Fig. 6(b), because for the former, the anisotropy varies smoothly with angle, as expected intuitively.

The matrix representing the Schrödinger equation for the electron in the Born–Oppenheimer basis is

$$i\hbar\,\frac{d}{dt}\,\underline{c}(t)=(\underline{h}_{\mathrm{el}}-\dot{\Phi}_{\mathrm{Ar}}\underline{L}_z)\underline{c}(t),\quad \underline{h}_{\mathrm{AC}}=-\dot{\Phi}_{\mathrm{Ar}}\underline{L}_z, \tag{5}$$

where the additional angular coupling term, $\underline{h}_{\mathrm{AC}}$ arises because the basis functions rotate with the triatomic plane over the course of a collision. The full Hamiltonian matrix in the Born–Oppenheimer representation is given by

$$\underline{h}_{\mathrm{el}}+\underline{h}_{\mathrm{AC}}=\begin{bmatrix}\epsilon_{\mathrm{ip}}(R_{\mathrm{Ar}},\Theta_{\mathrm{Ar}}) & i\dot{\Phi}_{\mathrm{Ar}}\hbar\\ -i\dot{\Phi}_{\mathrm{Ar}}\hbar & \epsilon_{\mathrm{op}}(R_{\mathrm{Ar}},\Theta_{\mathrm{Ar}})\end{bmatrix}. \tag{6}$$

We orient the NO molecule in the laboratory frame, fixing the value of $\beta$ at 0 or $\pi/2$, and use a straight-line trajectory for the Ar. To gain insight into the collision dynamics we examine individual trajectories. To calculate orientation cross sections we average the results of individual trajectories over impact parameter, $b$, and azimuthal angle, $\Phi_{\mathrm{Ar}}^{L}$.

We use a collision energy of 35 meV, easily attained in a crossed-beam apparatus using a jet source for Ar.

## IV. PICTURES OF EVOLUTION OF ELECTRONIC ANGULAR MOMENTUM

To gain insight into the mechanism of the Λ-doublet transition, we monitor the evolution of the expectation value of the electronic angular momentum vector, $\langle\Lambda\rangle$, for several representative types of trajectories. So that we can easily see the time-evolution of $\langle\Lambda\rangle$, we choose the initial electronic state to be $|\Lambda\rangle=|+1\rangle$. The same basic physics is involved for an initial $\Pi_x$ state; however, $\langle\Lambda\rangle=0$ for this state and so its behavior is not as readily observable.

### A. Parallel orientation

Consider the case where $\mathbf{v}_{\rm rel}$ is parallel to the diatomic axis, as shown in Fig. 1(a). A vector evolution diagram for this case is shown in Fig. 7(a). To generate this trajectory, the NO molecule is oriented along the $Z^L$ axis by setting $\beta=0°$, the azimuthal angle, $\Phi^L_{\rm Ar}$, is arbitrary, and we choose $b=3$ a.u. We see that $\langle\Lambda\rangle$ changes both in magnitude and direction over the course of the trajectory; however, it is hard to discern its actual behavior. Figure 7(b) shows a plot of $\langle\Lambda\rangle$ vs time, in which we see $\langle\Lambda\rangle$ starts out $+1$ and then oscillates between $\pm1$, with a rate that increases as the distance between the diatomic and Ar decreases. These oscillations in Λ are a kind of restricted precession. As mentioned in the introduction, if the NO molecule were a single atom, then the electronic orbital-angular momentum, $\langle\mathbf{L}\rangle$, would lock onto and precess about the $\mathbf{R}_{\rm Ar}$ axis. However, since this angular momentum is already strongly locked onto the NO axis, only $\langle L_Z\rangle=\langle\Lambda\rangle$ is relevant, and the precession about the $\mathbf{R}_{\rm Ar}$ axis is restricted to oscillation along the NO axis. For this particular trajectory, $\langle\Lambda\rangle$ ends up $-1$, indicating a probability of 1 for transition to the $\langle\Lambda\rangle=-1$ state.

Another way of looking at the collision process is to plot the probability of being in the rotating triatomic basis state, $\phi_{\rm ip}$, over time, shown in Fig. 7(c). We see that the electronic state starts in a 50:50 mixture of $\phi_{\rm ip}$ and $\phi_{\rm op}$, and stays exactly in that mixture. We can understand this behavior by examining the magnitudes of the electrostatic and angular couplings, shown in Fig. 7(d). This plot shows that the anisotropy of the potential, which causes $\langle\Lambda\rangle$ to oscillate, increases as $R_{\rm Ar}$ decreases, causing the observed increase in oscillation rate with decreasing $R_{\rm Ar}$. We also see that for this particular trajectory, there is no angular coupling, for the triatomic frame remains space-fixed throughout the collision. Since there is no coupling between the triatomic basis functions, the electronic state can be written as a linear combination of these two basis states with probability amplitudes that are constant, but phases which depend on the energy of the basis functions,

$$\Psi(t)=c_{\rm ip}(0)|\phi_{\rm ip}\rangle e^{-i\epsilon_{\rm ip}t/\hbar}+c_{\rm op}(0)|\phi_{\rm op}\rangle e^{-i\epsilon_{\rm op}t/\hbar}. \tag{7}$$

These phases oscillate at different rates, resulting in an oscillation of the state between $|\Lambda\rangle=|\pm1\rangle$, as shown in Fig. 7(b). Since all trajectories in which $\mathbf{v}_{\rm rel}$ is parallel to the diatomic axis have no angular coupling, they all show this behavior, differing only in the oscillation rate.

### B. Perpendicular orientation

Consider now the case where $\mathbf{v}_{\rm rel}$ is perpendicular to the diatomic axis, as in Fig. 1(b). Now the azimuthal angle, $\Phi^L_{\rm Ar}$, about $\mathbf{v}_{\rm rel}$ affects the collision dynamics, for it characterizes whether the Ar atom passes by the O-end, the N-end, or somewhere in between the two ends of the NO molecule. We observe two general types of behavior for this case, distinguished by whether or not the triatomic is nearly linear at the distance of closest approach.

Figure 8(a) shows a vector evolution diagram for a trajectory with impact parameter of 3 a.u. and an azimuthal angle, $\Phi^L_{\rm Ar}$, of 40°. We see that $\langle\Lambda\rangle$ starts out $+1$ and then oscillates between $\pm1$, with a rate that increases as the distance between the diatomic and Ar decreases. For this particular trajectory, it also happens to end up $-1$, indicating a probability of 1 for transition. A plot of $|c_{\rm ip}|^2$ vs $t$, shown in Fig. 8(c), indicates that the electronic state starts in a 50:50 mixture of $\phi_{\rm ip}$ and $\phi_{\rm op}$, and pretty much stays in that mixture, though not as well as in the case of parallel orientation shown in Fig. 7(c). We can understand the behavior for this trajectory by examining the magnitudes of the electrostatic and angular couplings, shown in Fig. 8(d). Here we see that both the anisotropy of the potential, and the angular coupling increase as $R_{\rm Ar}$ decreases; however, the anisotropy is always much larger than the angular coupling.

Consider now the case where $\mathbf{v}_{\rm rel}$ is again perpendicular to the diatomic axis, but the triatomic is nearly linear at the distance of closest approach. Figure 9(a) shows a vector evolution diagram for this case, where $\Phi^L_{\rm Ar}=10°$, and again $b=3$ a.u. We see that in the first half of the collision, $\langle\Lambda\rangle$ oscillates between $\pm1$, while in the second half it oscillates within a smaller range. In Fig. 9(b) we plot $\langle\Lambda\rangle$ vs time. For this particular trajectory, it ends up $-0.5$, indicating a probability for transition of about 3/4. Figure 9(c) shows the probability of being in the rotating triatomic basis state, $\phi_{\rm ip}$, over time. We see that the electronic state again starts in a 50:50 mixture of $\phi_{\rm ip}$ and $\phi_{\rm op}$, and that this ratio is reasonably constant as the Ar approaches, but that at the distance of closest approach it abruptly changes to a new value which remains fairly constant for the rest of the collision. Examining the magnitudes of the electrostatic and angular couplings shown in Fig. 9(d), we see that the anisotropy has a dip at the distance of closest approach, which is due to symmetry, resulting in a situation where the angular coupling overtakes the anisotropy. We interpret this trajectory as having an orbital following region, in which the anisotropy is larger than the angular coupling, inside of which is a partial unlocking region, in which the angular coupling is larger than the anisotropy, and then another orbital following region.

### C. Other impact parameters

In the pictures described above, the impact parameter was 3 a.u. Figure 10 shows how the transition probability varies with impact parameter for each of the three cases. We

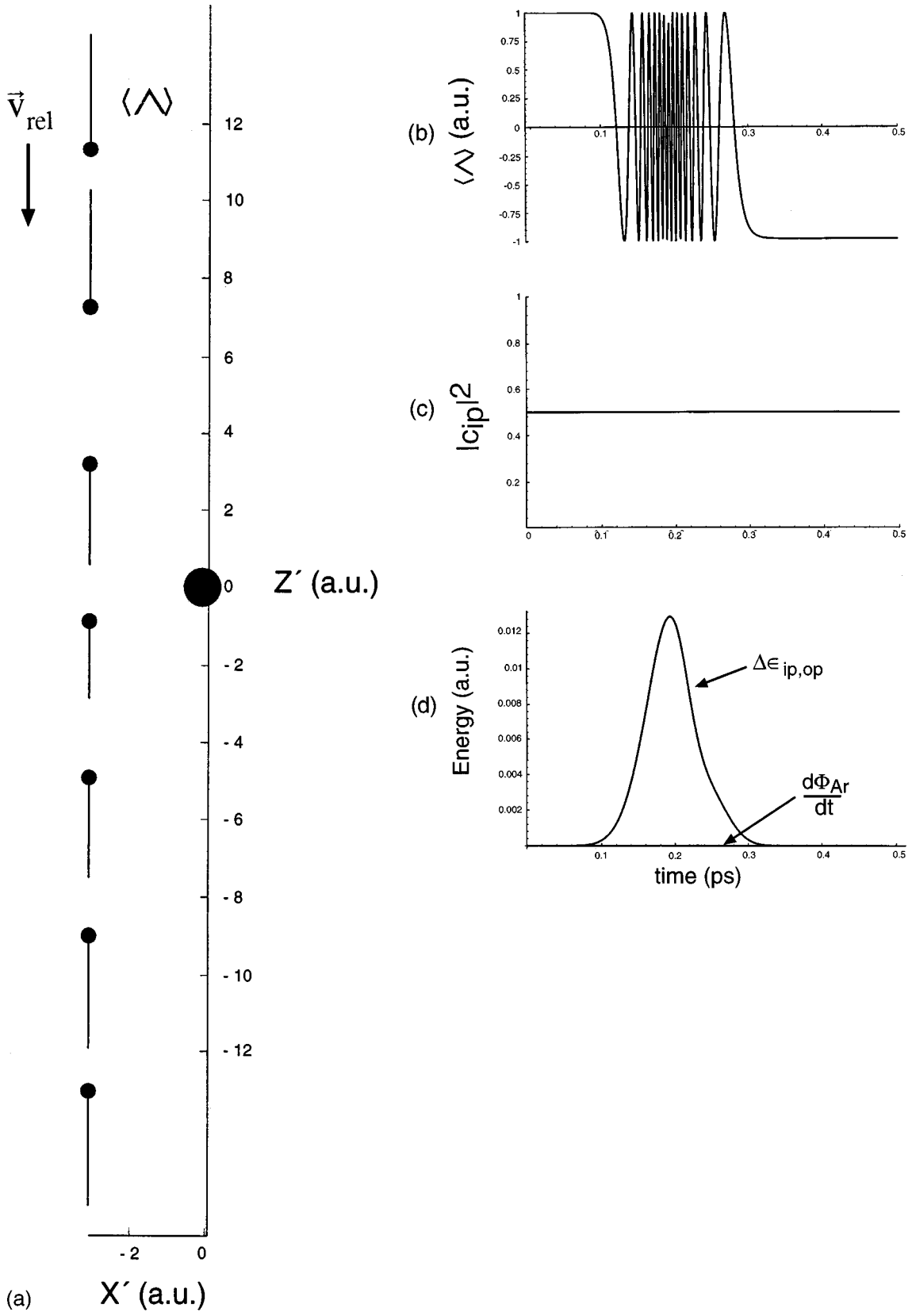


FIG. 7. (a) Vector evolution diagram for a trajectory where $\mathbf{v}_{rel}$ is parallel to the diatomic axis. The initial electronic state is $\langle\Lambda\rangle = +1$ and the impact parameter is 3 a.u. The Ar atom is located at the origin, and the NO molecule travels from the top to the bottom of the page. Although it can be seen that $\langle\Lambda\rangle$ oscillates along the internuclear axis, this type of picture does not allow for a detailed view of its behavior. To better see the behavior of $\langle\Lambda\rangle$, (b) shows $\langle\Lambda\rangle$ vs time. Note that it oscillates between $\pm 1$, with a rate that increases as the distance between NO and Ar decreases. To see what is happening from the point of view of the triatomic frame, (c) shows $|c_{ip}|^2$ which does not change at all. These behaviors can be understood by (d) which shows the anisotropy of the potential (solid line) and the angular coupling term (dotted line) which is zero throughout the trajectory. For all parallel trajectories, the angular coupling term is zero.

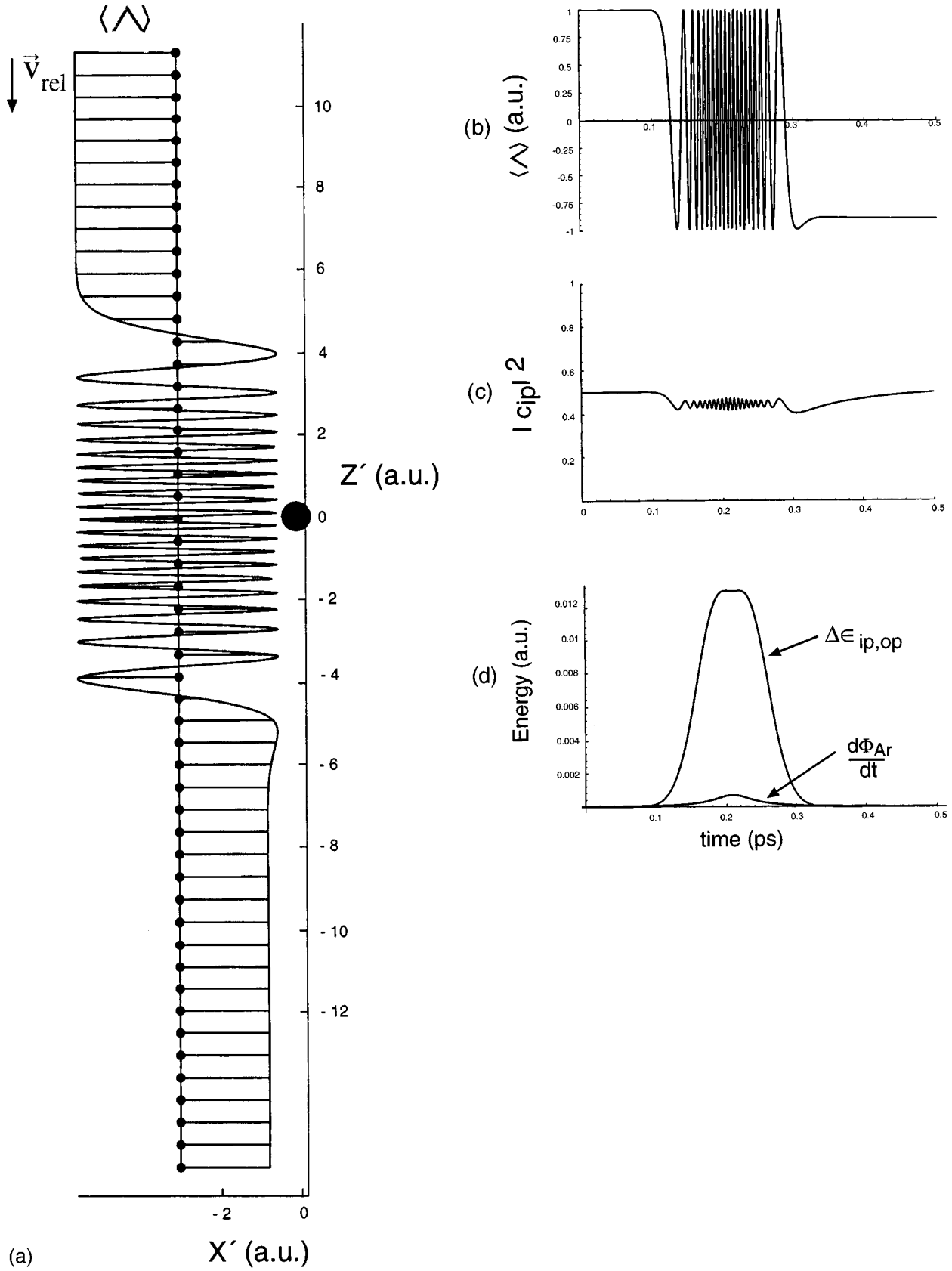


FIG. 8. (a) Vector evolution diagram for a trajectory where $\mathbf{v}_{rel}$ is perpendicular to diatomic axis. The initial electronic state is $\langle\Lambda\rangle=+1$, the impact parameter is 3 a.u., and the azimuthal angle, $\Phi_{Ar}^{L}$, is 40°, meaning at the distance of closest approach, Ar is slightly closer to the O atom than the N atom (see Fig. 5). (b) shows $\langle\Lambda\rangle$ as a function of time. In this case, $\langle\Lambda\rangle$ oscillates between $\pm1$. (c) shows $|c_{ip}|^2$, which is nearly constant until the atoms are close, where it exhibits a small amplitude of oscillation about the initial value. These behaviors can be understood from (d) which shows both the anisotropy and the angular coupling as functions of time. We see that there is angular coupling in this case, which is largest at the distance of closest approach. However, in the interaction region, these large angle trajectories are still dominated by the anisotropy, with the angular coupling term a small perturbation.

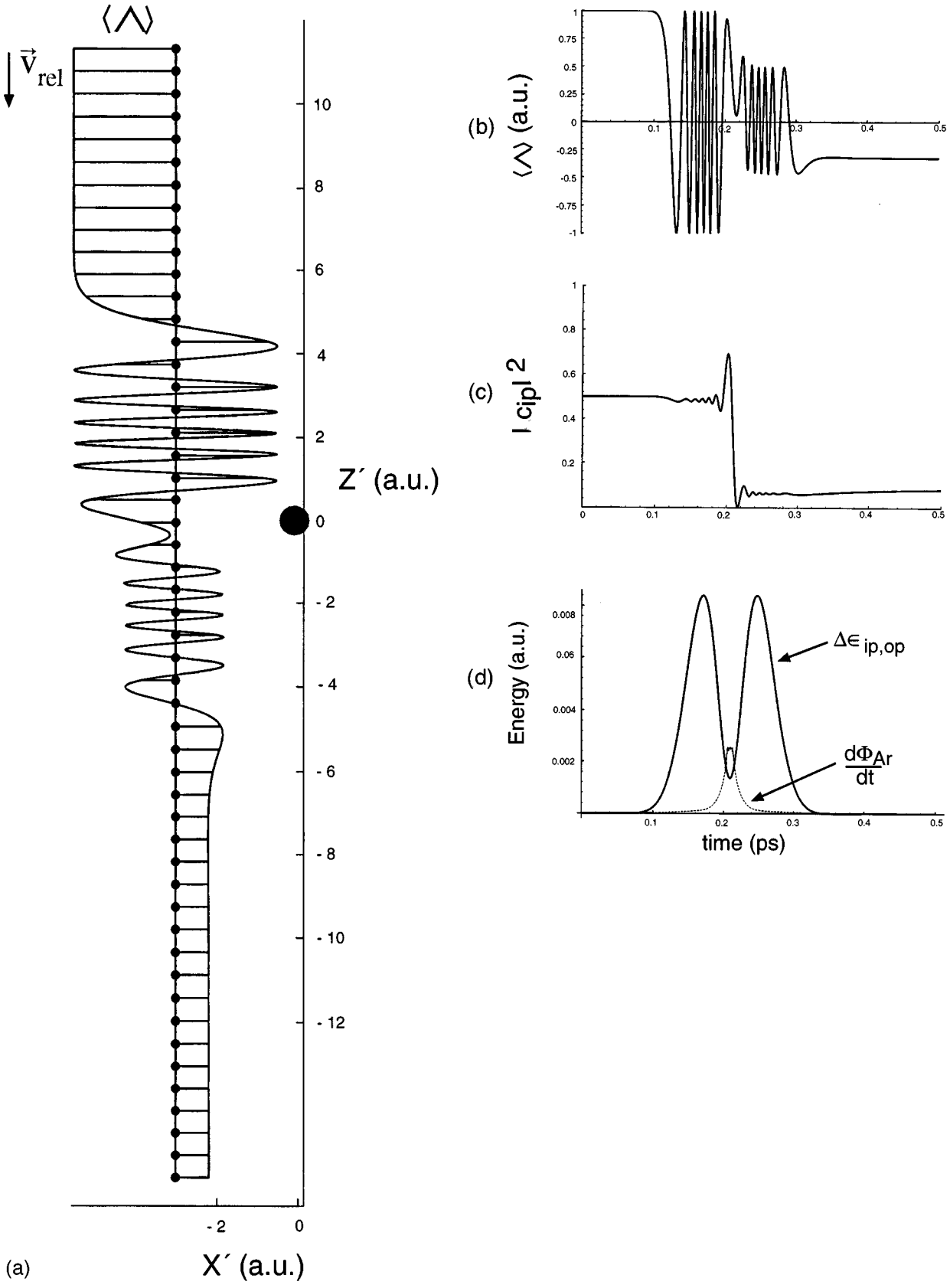


FIG. 9. Same as Fig. 8, except the azimuthal angle, $\Phi^L_{Ar}$, is 10°, meaning that at the distance of closest approach, Ar is nearly along the nuclear axis, closer to the O-end of the molecule. For these trajectories, which have a nearly linear triatomic configuration at the distance of closest approach, we see that $\langle\Lambda\rangle$ oscillates between $\pm 1$ in the first half of the interaction region, as in the previous cases, but, for the latter half of the interaction region, it oscillates with a smaller amplitude. The proportion of $\phi_{ip}$ character changes for the latter half of the collision. In this trajectory, the anisotropy of the potential actually decreases at the distance of closest approach, resulting in a situation where the angular coupling term is greater than the anisotropy.

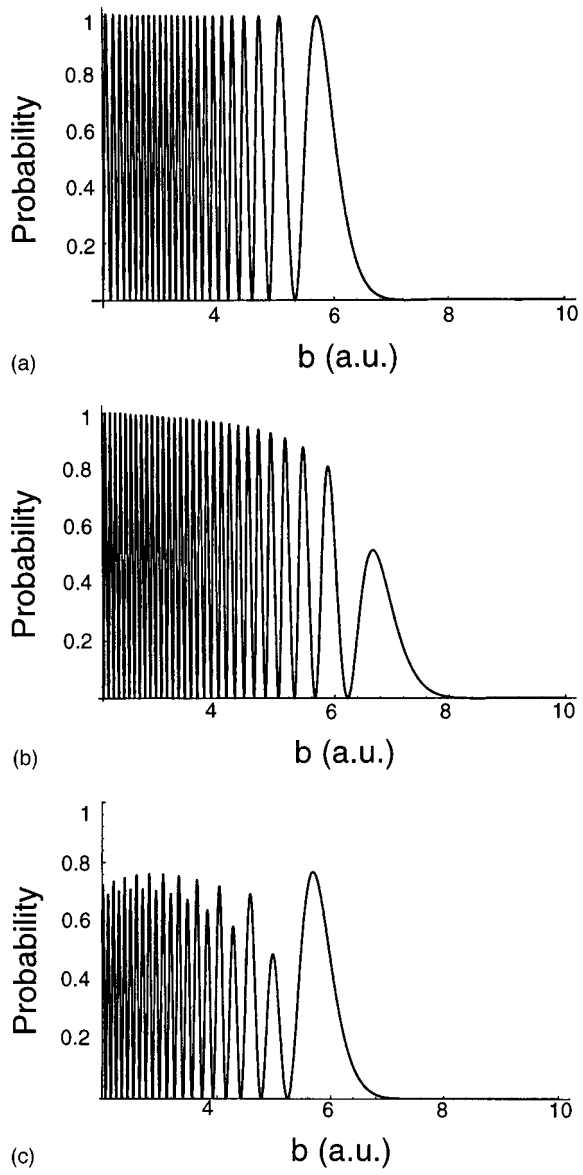


FIG. 10. Plots of probability (not weighted by impact parameter) vs $b$ for transition from an initial $\Lambda=+1$ state to a final $\Lambda=-1$ state for three cases; (a) parallel alignment, (b) perpendicular alignment with $\Phi_C^L=40°$, and (c) perpendicular alignment with $\Phi_{\mathrm{Ar}}^L=10°$. The trajectories comprising these three plots differ in the relative magnitudes of angular and electrostatic coupling; for (a) the angular coupling is always zero; for (b) the angular coupling is nonzero but always less than electrostatic coupling; for (c) the angular coupling overtakes the electrostatic coupling near the distance of closest approach.

see that for the case of parallel orientation, shown in Fig. 10(a), the transition probability oscillates between 0 and +1 for all values of $b$. Maxima in the transition probability correspond to impact parameters at which $\langle\Lambda\rangle$ undergoes a half-integral number of oscillations. For the case of perpendicular orientation and $\Phi_{\mathrm{Ar}}^L=40°$ the transition probability oscillates between 0 and some other number which decreases with increasing $b$, due to the angular coupling being an increasingly large fraction of the anisotropy. Figure 10(c), corresponding to perpendicular orientation and $\Phi_{\mathrm{Ar}}^L=10°$, is most interesting, as there is a second frequency of oscillation superimposed upon the first. This behavior is due to the presence of a partial unlocking region.

## V. EFFECT OF ORIENTATION ON CROSS SECTIONS

We now calculate the cross sections for two types of collision-induced transition; for transition between Λ-doublet states where the molecule starts out in $\Pi_x$ and ends up in $\Pi_y$, and for transition between states of definite Λ, where the molecule starts out in $\Lambda=+1$ and ends up in $-1$. We model a hypothetical three-vector correlation experiment in which crossed atomic and molecular beams are used to define a relative velocity vector, $\mathbf{v}_{\mathrm{rel}}$, a strong electric field, directed in the plane of the macroscopic beams, is used to orient the molecule either parallel or perpendicular to $\mathbf{v}_{\mathrm{rel}}$, and a laser beam is used to prepare the initial electronic state. To prepare the $\Pi_x$ Λ-doublet state, the laser is linearly polarized and propagates in a direction perpendicular to the atomic and molecular beams, while to prepare the $\Lambda=+1$ state, the laser beam is circularly polarized and propagates along the direction of the diatomic axis.

### A. Transition between ±1 states

The circularly polarized laser beam, propagating along the direction of the diatomic axis, prepares the NO molecule in the $|\Lambda\rangle=|+1\rangle$ state. Collision carries this initial state into a corresponding final state, $|f\rangle$, so the probability of transition into the $|-1\rangle$ state is given by

$$P(\beta,b,\Phi_{\mathrm{Ar}}^L)=|\langle -1|f\rangle|^2. \tag{8}$$

This probability depends on the orientation angle, $\beta$, the impact parameter, $b$, and the azimuthal angle, $\Phi_{\mathrm{Ar}}^L$. To calculate the orientation cross section, we fix $\beta$ and average the probability over $b$ and $\Phi_{\mathrm{Ar}}^L$,

$$\sigma(\beta)=\int_0^{2\pi} d\Phi_{\mathrm{Ar}}^L \int_0^{\infty} bdbP(\beta,b,\Phi_{\mathrm{Ar}}^L). \tag{9}$$

For the case of $\mathbf{v}_{\mathrm{rel}}$ parallel to the diatomic axis ($\beta=0°$), the distribution of impact parameters is cylindrically symmetric about $\mathbf{v}_{\mathrm{rel}}$. Therefore the orientation cross section, $\sigma(0)$, which we call $\sigma_{\parallel}$, is given by

$$\sigma_{\parallel}=\int_0^{\infty} P(\beta=0,b)2\pi bdb. \tag{10}$$

The integral over $b$ is summed numerically from $b=0$ to 10 a.u. with steps of 0.2 a.u. A plot of $P(0,b)$ vs $b$ was shown in Fig. 10(a).

For the case of $\mathbf{v}_{\mathrm{rel}}$ perpendicular to the diatomic axis ($\beta=\pi/2$), the distribution of impact parameters is not cylindrically symmetric about $\mathbf{v}_{\mathrm{rel}}$. We obtain the orientation cross section, $\sigma(0)$, which we call $\sigma_{\perp}$, by summing numerically first over $b$ as above, and then over $\Phi_{\mathrm{Ar}}^L$ in steps of 10°. Plots of $P(\pi/2,b,\Phi_{\mathrm{Ar}}^L)$ vs $b$ for two values of $\Phi_{\mathrm{Ar}}^L$ were shown in Figs. 10(b) and 10(c).

Plots of probability averaged over $b$ as a function of $\Phi_{\mathrm{Ar}}^L$ are shown in Fig. 11(a) for the two cases of parallel and perpendicular orientation. The area under each curve is equal

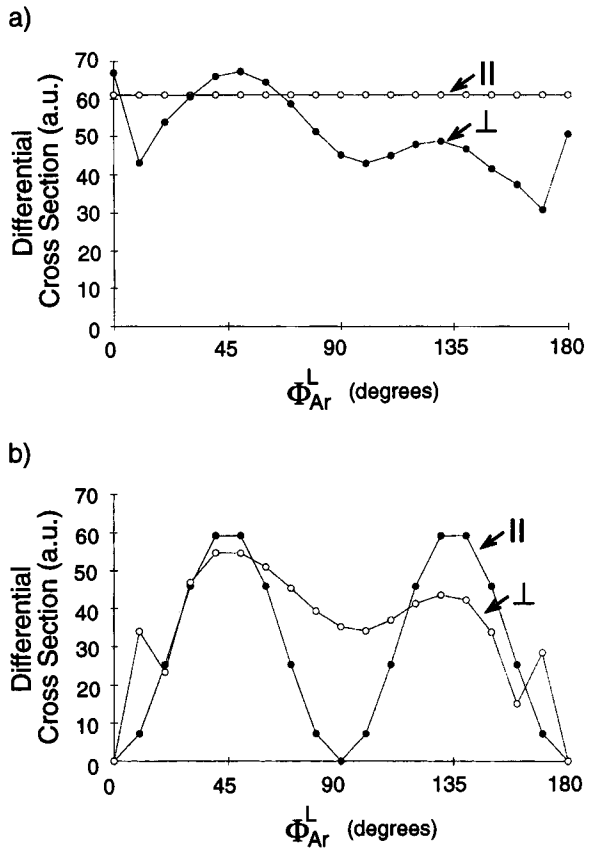


FIG. 11. Differential cross section for parallel (closed circles) and perpendicular (open circles) alignment as a function of azimuthal angle, $\Phi^L_{\mathrm{Ar}}$, (a) for transition from an initial $\Lambda=+1$ state to the $\Lambda=-1$ state, and (b) for an initial $\Pi_X$ state to the $\Pi_Y$ state. The area under each curve corresponds to the integrated cross section for that alignment. We see that transition from $\Lambda=+1$ to $\Lambda=-1$ is preferentially produced with perpendicular alignment, while transition from $\Pi_X$ to $\Pi_Y$ is preferentially produced with parallel alignment.

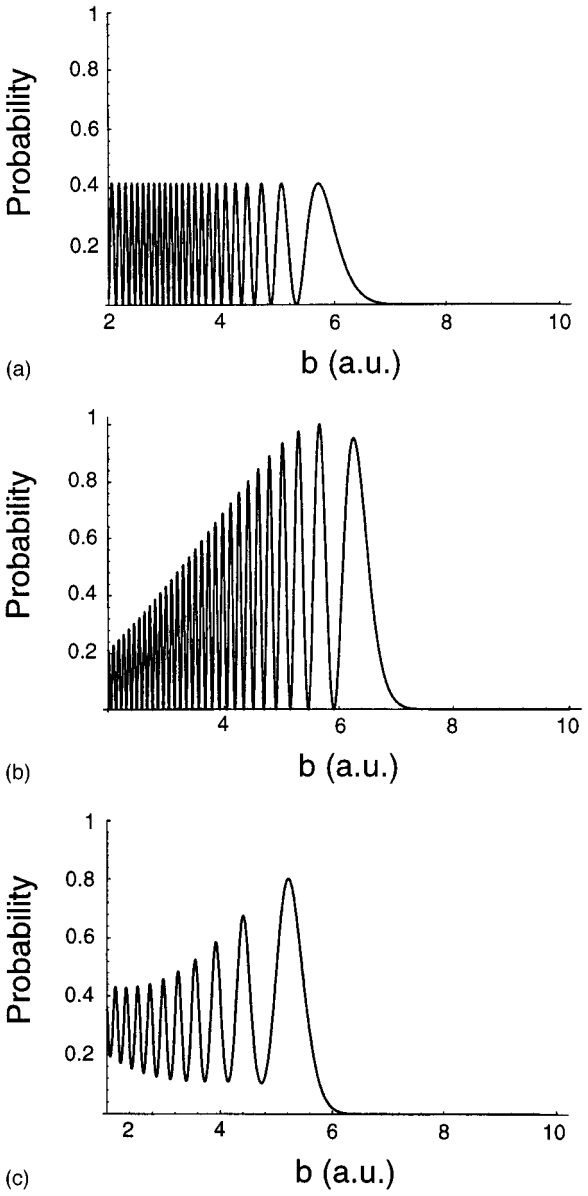


FIG. 12. Same as Fig. 10 except that the transition occurs from an initial $\Pi_X$ state to the $\Pi_Y$ state.

to the orientation cross section. It is evident that $\sigma_{\parallel}$ is greater than $\sigma_{\perp}$. We find $\sigma_{\parallel}=61$ a.u.$^2$ and $\sigma_{\perp}=51$ a.u.$^2$, giving an orientation effect, $\sigma_{\parallel}/\sigma_{\perp}$, of 1.20. We are unable to give a simple explanation for this result since it is obtained by averaging over individual trajectories differing in behavior.

### B. Transitions between Λ-doublet states

In this version of the experiment, a linearly polarized laser is used to prepare an initial $\Pi_x$ state. The laser beam propagates along the $Y^L$ axis and is polarized perpendicular to the diatomic axis. Collision carries this initial state into a corresponding final state, $|f\rangle$, so the probability of transition into the $|\Pi_y\rangle$ state is given by

$$P(\beta,b,\Phi^L_{\mathrm{Ar}})=|\langle\Pi_y|f\rangle|^2 \tag{11}$$

and depends on the orientation angle, $\beta$, the impact parameter, $b$, and the azimuthal angle, $\Phi^L_{\mathrm{Ar}}$. To calculate the orientation cross section, we fix $\beta$ and average the probability over $b$ and $\Phi^L_{\mathrm{Ar}}$, as described in Sec. IV C:

$$\sigma(\beta)=\int_0^{2\pi} d\Phi^L_{\mathrm{Ar}}\int_0^{\infty} bdbP(\beta,b,\Phi^L_{\mathrm{Ar}}). \tag{12}$$

In this case, the transition probability depends on $\Phi^L_{\mathrm{Ar}}$ for all values of $\beta$, so the orientation cross sections are obtained by summing numerically over both $b$ and $\Phi^L_{\mathrm{Ar}}$. Plots analogous to those shown in Fig. 10 are shown in Fig. 12. Comparison of Figs. 10(a) and 12(a) shows similar behavior in that both trajectories exhibit an oscillation with fixed amplitude. However, the value of that amplitude is smaller for the case of an initial $\Pi_X$ state. Inspection of trajectories for other values of $\Phi^L_{\mathrm{Ar}}$ shows that the amplitude of oscillation changes with $\Phi^L_{\mathrm{Ar}}$, attaining its maximum, $+1$, for $\Phi^L_{\mathrm{Ar}}=45°$.

It is interesting to explore this case a bit further by looking at a particular trajectory. Figure 13 shows a plot of transition probability vs time for the case of parallel orientation, $b=3$ a.u., and $\Phi^L_{\mathrm{Ar}}=45°$. Note how the probability for transition to the $\Pi_Y$ state oscillates between 0 and 1, i.e., the diatomic electronic state oscillates between $\Pi_X$ and $\Pi_Y$ as

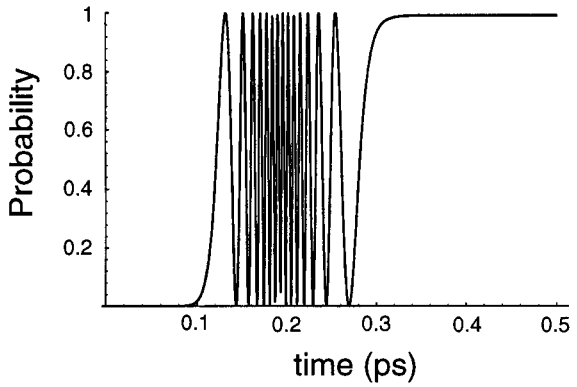


FIG. 13. Probability for transition from an initial $\Pi_X$ state to the $\Pi_Y$ state along the course of a single trajectory with $b=3$ a.u., parallel alignment, and $\Phi_{\rm Ar}^L=45°$. The observed oscillation of probability between 0 and 1 implies the electronic state oscillates between $\Pi_X$ and $\Pi_Y$.

the Ar atom passes through the interaction region. This is a simple consequence of Eq. (7), as we will explain in the next section.

We now consider the case of perpendicular orientation. Figures 12(b) and 12(c) show the probability for transition to the $\Pi_Y$ state as a function of $b$ for the case of perpendicular orientation, for two values of $\Phi_{\rm Ar}^L$, 40° and 10°.

Plots of probability averaged over $b$ as a function of $\Phi_{\rm Ar}^L$ are shown in Fig. 11(b) for both orientations. The area under each curve is equal to the orientation cross sections. It is evident that now $\sigma_\parallel$ is less than $\sigma_\perp$. We find $\sigma_\parallel = 30.5$ a.u.$^2$ and $\sigma_\perp = 36.6$ a.u.$^2$, giving an orientation effect, $\sigma_\parallel/\sigma_\perp$, of 0.833. Thus the orientation effect is the inverse of that found for transition between the $\pm1$ states.

## VI. ANALYTIC SOLUTIONS

All the above vector evolution diagrams were obtained by numerical solution of the coupled equations [Eq. (5)]. An alternative approach is to solve the equations analytically. We can exactly solve the equations for the case of parallel orientation; however, we need to make further approximations for the case of perpendicular orientation.

### A. Parallel orientation

For this case there is no angular coupling as the triatomic frame is space fixed. The matrix representation of the Hamiltonian in the ip–op basis is thus

$$\underline{h}_{\rm el}+\underline{h}_{\rm AC}=\begin{bmatrix}\epsilon_{\rm ip}(R_{\rm Ar},\Theta_{\rm Ar}) & 0\\ 0 & \epsilon_{\rm op}(R_{\rm Ar},\Theta_{\rm Ar})\end{bmatrix} \tag{13}$$

and the solution to the coupled equations for this Hamiltonian is

$$c_{\rm ip}(t)=c_{\rm ip}(0)e^{-i\int_0^t\epsilon_{\rm ip}dt'/\hbar},\quad c_{\rm op}(t)=c_{\rm op}(0)e^{-i\int_0^t\epsilon_{\rm op}dt'/\hbar}. \tag{14}$$

We first consider transition from the $\Lambda=+1$ state to the $\Lambda=-1$ state. We label the probability amplitude for being in each of these two diatomic frame basis functions $d_+$ and $d_-$, respectively. The representation of the electronic state in the diatomic $\Lambda=\pm1$ basis is related to the representation in the triatomic Born–Oppenheimer basis by two unitary transformations, the first corresponding to rotation of the triatomic frame into the diatomic frame by the angle $\Phi_{\rm Ar}^L$, the second to transformation from the diatomic $\Pi_{X,Y}$ representation to the diatomic $\Lambda$ representation,

$$\underline{c}=\underline{U}\,\underline{V}\,\underline{d}_\pm, \tag{15a}$$

where

$$\underline{c}=\begin{pmatrix}c_{\rm ip}\\ c_{\rm op}\end{pmatrix},\quad \underline{d}_\pm=\begin{pmatrix}d_+\\ d_-\end{pmatrix},\quad \underline{U}=\begin{pmatrix}-\frac{1}{\sqrt{2}} & \frac{1}{\sqrt{2}}\\ \frac{i}{\sqrt{2}} & \frac{i}{\sqrt{2}}\end{pmatrix},$$

$$\underline{V}=\begin{pmatrix}e^{-i\Phi_{\rm Ar}^L} & 0\\ 0 & e^{i\Phi_{\rm Ar}^L}\end{pmatrix}. \tag{15b}$$

Then $\underline{d}_\pm$ at any time $t$ is given by

$$\underline{d}_\pm(t)=\underline{V}^\dagger\underline{U}^\dagger\begin{pmatrix}e^{-i\int_0^t\epsilon_{\rm ip}dt'/\hbar} & 0\\ 0 & e^{-i\int_0^t\epsilon_{\rm op}dt'/\hbar}\end{pmatrix}\underline{U}\,\underline{V}\,\underline{d}_\pm(0). \tag{16}$$

If the molecule starts out in the state $\Lambda=+1$, the probability of transition to the $\Lambda=-1$ state at time $t$ is given by $|d_-(t)|^2$ where

$$d_-(t)=e^{-i\Phi_{\rm Ar}^L}\tfrac{1}{2}(-e^{-i\int_0^t\epsilon_{\rm ip}dt'/\hbar}+e^{-i\int_0^t\epsilon_{\rm op}dt'/\hbar}). \tag{17}$$

By making the transformation of variables,

$$\epsilon_{\rm av}=\frac{\epsilon_{\rm ip}+\epsilon_{\rm op}}{2};\quad \epsilon_{\rm dif}=\frac{\epsilon_{\rm ip}-\epsilon_{\rm op}}{2}, \tag{18}$$

Eq. (17) becomes

$$d_-(t)=ie^{-i(\Phi_{\rm Ar}^L+\int_0^t\epsilon_{\rm av}dt'/\hbar)}\sin\left(\int_0^t\epsilon_{\rm dif}dt'/\hbar\right). \tag{19}$$

Thus the probability for transition, $|d_-(t)|^2$, oscillates between 1 and 0 in the interaction region, with a rate that depends on $\Delta\epsilon_{\rm ip,op}$, which itself changes along the course of a trajectory. This result is in agreement with the computer-generated plot in Fig. 7(b). Trajectories differing in $b$ will show a difference only in the rate of oscillation, in agreement with the computer-generated plot in Fig. 10(a). Note also that the transition probability shows no dependence on $\Phi_{\rm Ar}^L$, in agreement with the computer-generated picture in Fig. 11(a).

Now we consider the case of a diatomic molecule in an initial $\Pi_X$ state, and calculate the probability for transition into the $\Pi_Y$ state. We label the coefficients for the $\Pi_X$, $\Pi_Y$ diatomic basis states $d_X$, $d_Y$, respectively. These states can be related to the (ip,op) states by three unitary transformations,

$$\underline{c}=\underline{U}\,\underline{V}\,\underline{U}^\dagger\underline{d}_{XY}, \tag{20a}$$

where

$$\underline{d}_{XY}=\begin{pmatrix} d_X \\ d_Y \end{pmatrix}. \tag{20b}$$

Following the method outlined above, we obtain the equation

$$\underline{d}_{XY}(t)=\underline{U}\,\underline{V}^{\dagger}\underline{U}^{\dagger}\begin{pmatrix} e^{-i\int_0^t \epsilon_{\rm ip}dt'/\hbar} & 0 \\ 0 & e^{-i\int_0^t \epsilon_{\rm op}dt'/\hbar} \end{pmatrix}\underline{U}\,\underline{V}\,\underline{U}^{\dagger}\underline{d}_{\pm}(0). \tag{21}$$

If the molecule starts out in $\Pi_X$, $[d_X(0)=1]$, the probability of transition to the $\Pi_Y$ state is then given by $|d_Y(t)|^2$ where

$$d_y(t)=-2i\,\sin(\Phi^L_{\rm Ar})\cos(\Phi^L_{\rm Ar})e^{-i\int_0^t \epsilon_{\rm av}dt'/\hbar} \times\sin\left(\int_0^t \epsilon_{\rm dif}dt'/\hbar\right). \tag{22}$$

Again we see that the probability oscillates with a frequency determined by $\Delta\epsilon_{\rm ip,op}$. But this time the amplitude of oscillation depends on $\Phi^L_{\rm Ar}$, which is constant for a given trajectory. This result agrees with the computer-generated result shown in Fig. 12(a), and the functional form of the oscillation with $\Phi^L_{\rm Ar}$ agrees with the computer-generated result shown in Fig. 11(b).

### B. Perpendicular orientation

In the case of perpendicular orientation, the Hamiltonian contains two terms, electrostatic coupling and angular coupling. To solve these equations analytically, we need to make further approximations. We divide perpendicular trajectories into two cases, those for which the angular coupling is always less than the electrostatic coupling in the interaction region, which occurs for $20°\leqslant\Phi^L_{\rm Ar}\leqslant 160°$, and those for which the angular coupling exceeds the electrostatic coupling in the interaction region, which occurs for $\Phi^L_{\rm Ar}<20°$ and for $\Phi^L_{\rm Ar}>160°$. [Two representative cases are shown in Figs. 8(d) and 9(d).]

We first consider the case of perpendicular orientation and $20°\leqslant\Phi^L_{\rm Ar}\leqslant 160°$. Since the angular coupling is always smaller than the electrostatic coupling, a perturbation method should work. However, because this case is analogous to the behavior seen for the Na+He system studied previously,[1] we omit the calculation in favor of a qualitative description of the dynamics. For trajectories with small impact parameter, the effect of angular coupling is negligible, and $\langle\Lambda\rangle$ oscillates between $\pm1$, as seen in Fig. 8(b). This behavior is similar to that seen for trajectories with parallel orientation, where there is no angular coupling. For larger impact parameter trajectories, however, the electrostatic coupling is weaker in the interaction region, allowing the effect of angular coupling to become more discernible. The result is a smaller amplitude of oscillation of $\langle\Lambda\rangle$, causing the probability for transition to decrease with impact parameter as seen in Fig. 10(b). This is the same behavior seen in the case of Na+He, where for such large impact parameter trajectories, the precession of $\langle\mathbf{L}\rangle$ about the rotating molecular axis was not fast enough to keep up, resulting in a change in the value of its projection onto that axis. The amplitude of oscillation of $\langle\Lambda\rangle$ for the molecular case studied here is analogous to the value of the projection of $\langle\mathbf{L}\rangle$ onto the rotating Na–He axis for the atomic case studied previously, i.e., in the atomic case, orbital-following corresponds to a fixed value of the projection of $\langle\mathbf{L}\rangle$ onto the Na–He axis, while for the molecular case orbital-following corresponds to a fixed amplitude of oscillation of $\langle\Lambda\rangle$.

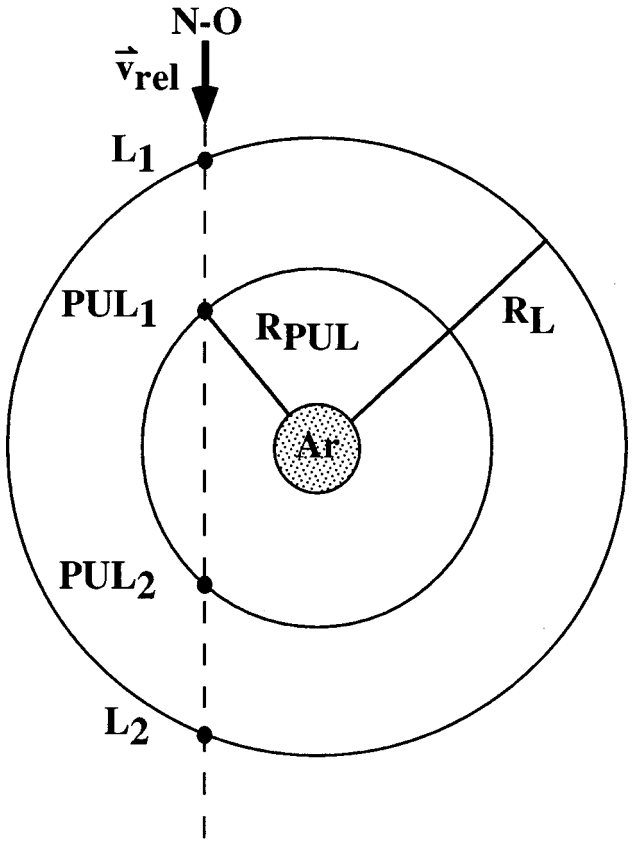


FIG. 14. Schematic of different collision zones for case of perpendicular alignment and either $\Phi^L_{\rm Ar}<20°$ or $\Phi^L_{\rm Ar}>160°$. The Ar atom is fixed at the origin and the NO molecule travels from the top of the page down. The intermolecular distance at which the NO molecule and the Ar atom start to interact strongly is called the locking radius, $R_L$. Thus we call the region outside $R_L$ the isolated molecule region, and the region inside $R_L$ the interaction region. We further divide the interaction region into two zones, the locking zone, corresponding to intermolecular distances between $R_L$ and $R_{\rm PUL}$ within which the electrostatic coupling is much stronger than the angular coupling, and the partial unlocking zone, corresponding to distances less than $R_{\rm PUL}$, within which the angular coupling overwhelms the electrostatic coupling. Along the course of the trajectory shown, the molecule starts out in the isolated molecule region, with $\langle\Lambda\rangle$ fixed, propagates through the locking region from point $L_1$ to $\rm PUL_1$, during which $\langle\Lambda\rangle$ oscillates rapidly, and then through the partial locking region from point $\rm PUL_1$ to $\rm PUL_2$, during which $\langle\Lambda\rangle$ changes only slightly. The $\langle\Lambda\rangle$ undergoes analogous behavior for the second half of the collision.

We now consider the case of perpendicular orientation where $\Phi^L_{\rm Ar}<20°$ or $\Phi^L_{\rm Ar}>160°$. In this case, the vector evolution diagrams display very different behavior from those in the atomic system. Since the electrostatic coupling overwhelms the angular coupling everywhere in the interaction region except near the distance of closest approach, we divide the interaction region into two zones, shown schematically in Fig. 14. Initially, when the Ar atom is far away, there

is no interaction between the NO and the Ar, and we neglect the electrostatic coupling terms in the Hamiltonian. At some distance which we call $R_L$, the locking radius, the electrostatic coupling overwhelms the angular coupling and we neglect angular coupling inside this region. As the Ar gets even closer, however, it reaches a distance, $R_{\mathrm{PUL}}$, which we call the partial unlocking radius, where the angular coupling exceeds the electrostatic coupling. Inside this region, it might seem reasonable to neglect electrostatic coupling entirely. However, we found that this approximation did not give the observed behavior seen in Fig. 9(b). Here it is necessary to consider the time-dependent competition between electrostatic and angular coupling. We did not find a simple model that gives accurate analytical expressions for this case.

## VII. CONCLUSION

We have obtained a picture of the mechanism for collision-induced Λ-doublet transitions in diatomic molecules, and showed how the expectation value $\langle\Lambda\rangle$ changes with time over the course of a collision for various collision geometries. For small enough distance between the diatomic and the perturber, the electrostatic coupling causes $\langle\Lambda\rangle$ to oscillate along the diatomic axis. This behavior is analogous to that seen for atoms, though in the latter case $\langle\mathbf{L}\rangle$ precesses about the rotating collision axis while in the former case it is so tightly locked onto the diatomic axis that it can only oscillate along that axis.

Usually, the electrostatic coupling increases with decreasing diatomic-perturber distance, resulting in an increase in the oscillation rate of $\langle\Lambda\rangle$. However, for certain collision geometries, we discovered a ''partial locking region,'' in which the electrostatic coupling actually decreases near the distance of closest approach. This behavior is due to symmetry, where $\epsilon_{\mathrm{ip}}$ and $\epsilon_{\mathrm{op}}$ are nearly degenerate at the distance of closest approach, and is specific to molecules; we do not encounter such a situation with atoms.

In addition to providing a physical picture of the collision, we have predicted an alignment effect of 1.2 for a hypothetical experiment in which oriented NO atoms collide with Ar. For this calculation we have suppressed the NO spin.

## ACKNOWLEDGMENTS

This research was supported by both the American Chemical Society-Petroleum Research Fund and by a William and Flora Hewlett Foundation Award of Research Corporation through grants to Eckerd College, and by NSF and ONR through grants to the College of William and Mary. We also want to gratefully acknowledge support by JILA where part of this work was completed. L.J.K. also thanks Steve Leone for valuable comments on the manuscript, and Neil York for help with computer programming.

[1] L. J. Kovalenko, S. R. Leone, and J. B. Delos, J. Chem. Phys. **91**, 6948 (1989).
[2] M. O. Hale and S. R. Leone, J. Chem. Phys. **79**, 3352 (1983); M. O. Hale, I. V. Hertel, and S. R. Leone, Phys. Rev. Lett. **53**, 2296 (1984); W. Bussert, D. Neuschäfer, and S. R. Leone, J. Chem. Phys. **87**, 3833 (1987); J. P. J. Driessen, C. J. Smith, and S. R. Leone, Phys. Rev. A **44**, R1431 (1991); J. Phys. Chem. **95**, 8163 (1991).
[3] M. P. I. Manders, J. P. J. Driessen, H. C. W. Beijerinck, and B. F. Verhaar, Phys. Rev. Lett. **57**, 1577 (1986); **57**, 2472 (1986); M. P. I. Manders, W. M. Ruyten, F.v.d. Beucken, J. P. J. Driessen, W. J. T. Veugelers, P. H. Kramer, E. J. D. Vredenbreght, W. B. M. van Hoek, G. J. Sandker, H. C. W. Beijerinck, and B. J. Verhaar, J. Chem Phys. **89**, 4777 (1988).
[4] J. J. van Leuken, F. H. W. van Amerom, J. Bulthuis, J. G. Snijders, and S. Stolte, J. Chem. Phys. **99**, 15 573 (1995).
[5] P. J. Dagdigian, in *The Chemical Dynamics and Kinetics of Small Radicals*, Advanced Series in Physical Chemistry, edited by K. Liu and A. Wagner (World Scientific, Singapore, 1995), Vol. 6, p. 315.
[6] Ch. Ottinger, R. Velasco, and R. N. Zare, J. Chem. Phys. **52**, 1636 (1970).
[7] K. Bergmann and W. Demtröder, J. Phys. B **5**, 1386 (1972).
[8] K. Bergmann, H. Klar, and W. Schlecht, Chem. Phys. Lett. **12**, 522 (1972).
[9] D. Poppe, Chem. Phys. Lett. **19**, 63 (1973).
[10] Ch. Ottinger, Chem. Phys. **1**, 161 (1973).
[11] H. Klar and M. Klar, J. Phys. B **8**, 129 (1975).
[12] D. Lemoine, G. C. Corey, M. H. Alexander, and J. Derouard, Chem. Phys. **118**, 357 (1987).
[13] R. A. Copeland and D. R. Crosley, J. Chem. Phys. **81**, 6400 (1984).
[14] I. J. Wysong, J. B. Jeffries, and D. R. Crosley, J. Chem. Phys. **94**, 7547 (1991).
[15] K. Schreel, J. Schleipen, A. Eppink, and J. J. ter Meulen, J. Chem. Phys. **99**, 8713 (1993).
[16] K. Schreel and J. J. Ter Meulen, J. Chem. Phys. **105**, 4522 (1996).
[17] A. R. Offer, M. C. Van Hemert, and E. F. Van Dishoeck, J. Chem. Phys. **100**, 362 (1994).
[18] A. D. Esposti, A. Berning, and H.-J. Werner, J. Chem. Phys. **103**, 2067 (1995).
[19] C. Dufour, B. Pinchemel, M. Douay, J. Schamps, and M. H. Alexander, Chem. Phys. **98**, 315 (1985).
[20] J. B. Norman and R. W. Field, J. Chem. Phys. **92**, 76 (1990).
[21] M. Bertojo, A. C. Cheung, and C. H. Townes, Astrophys. J. **208**, 914 (1976).
[22] P. Andresen, D. Häusler, and H. W. Lüff, J. Chem. Phys. **81**, 571 (1984)
[23] R. G. Macdonald and K. Liu, J. Chem. Phys. **91**, 821 (1989).
[24] R. Schinke and P. Andresen, J. Chem. Phys. **81**, 5644 (1984).
[25] P. J. Dagdigian, M. H. Alexander, and K. Liu, J. Chem. Phys. **91**, 839 (1989).
[26] S. M. Miller, D. C. Clary, A. Kliesch, and H.-J Werner, Mol. Phys. **83**, 405 (1994).
[27] P. Andresen, N. Aristov, V. Beushausen, D. Häusler, and H. W. Lülf, J. Chem. Phys. **95**, 5763 (1991).
[28] H. Joswig, P Andresen, and R. Schinke, J. Chem. Phys. **85**, 1904 (1986).
[29] G. C. Corey and M. H. Alexander, J. Chem. Phys. **85**, 1904 (1986).
[30] A. G. Suits, L. S. Bontuyan, P. L. Houston, and B. J. Whitaker, J. Chem. Phys. **96**, 8618 (1992); L. S. Bontuyan, A. G. Suits, P. L. Houston, and B. J. Whitaker, J. Phys. Chem. **97**, 6342 (1993).
[31] S. D. Jons, J. E. Shirley, M. T. Vonk, C. F. Giese, and W. R. Gentry, J. Chem. Phys. **97**, 7831 (1992); **105**, 5397 (1996).
[32] M. H. Alexander, J. Chem. Phys. **99**, 7725 (1993).
[33] B. Friedrich, D. R. Herschbach, J-M. Rost, H-G. Rubahn, M. Renger, and M. Verbeek, J. Chem. Soc. Faraday Trans. **89**, 1539 (1993).
[34] G. Herzberg, *Molecular Spectra and Molecular Structure*, 2nd ed. (Van Nostrand Reinhold, New York, 1950), Vol. 1, Appendix.
[35] G. C. Nielson, G. A. Parker, and R. T Pack, J. Chem. Phys. **66**, 1396 (1977). Note that there is a misprint in their value of $B_{nl}^{d'}$ which should read $0.113\,436\times10^{-2}$, rather than $0.133\,436\times10^{-2}$.